Journal of Materials Chemistry A

Accepted Manuscript

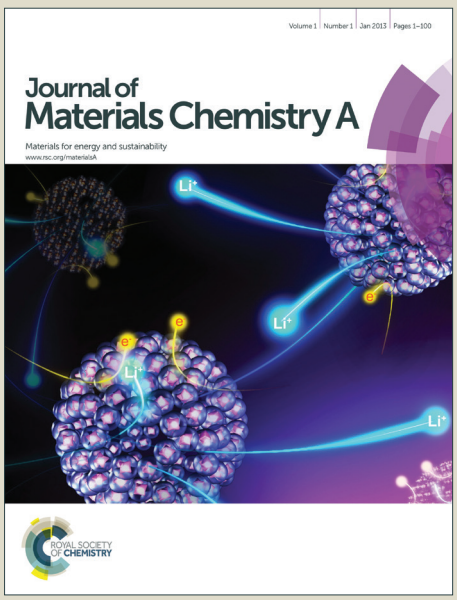

ROYAL SOCIETY OF CHEMISTRY

www.rsc.org/materialsA

Cite this: DOI: 10.1039/c0xx00000x

www.rsc.org/xxxxxx

ARTICLE TYPE

Enhanced electrochemical performance of novel K-doped Co_3O_4 as anode material for secondary lithium-ion batteries

Ly Tuan Anh[1], Alok Kumar Rai[1], Trang Vu Thi, Jihyeon Gim, Sungjin Kim, Vinod Mathew and Jaekook Kim

Received (in XXX, XXX) Xth XXXXXXXXX 20XX, Accepted Xth XXXXXXXXX 20XX
DOI: 10.1039/b000000x

K-doped Co_3O_4 was prepared by solvothermal method in polyol medium, followed by annealing at a low temperature of 400 °C for 5 h. The obtained samples were characterized by Synchrotron X-ray diffraction pattern, field-emission Scanning Electron Microscopy, Energy-Dispersive X-ray Spectroscopy, field-emission transmission electron microscopy and high-resolution Transmission Electron Microscopy. Synchrotron XRD analysis demonstrates that the K^+ ion doping caused no change in the phase structure, and highly crystalline $K_xCo_{3-x}O_{4-\delta}$ (x = 0.08) powder without any impurity was obtained. When applied as anode materials, the K^+-doped Co_3O_4 electrode exhibits much better rate capability and cycling stability, and could retain a charge capacity of 351.3 mAh g^{-1} at 3 C, while undoped Co_3O_4 exhibits only 144.3 mAh g^{-1} at the same rate. In addition, electrochemical impedance spectroscopy also reveals that the K^+-doped Co_3O_4 electrode has the highest electronic conductivity compared to an undoped sample. However, the improvement in the doped sample is due to the influence of K^+ ions on the increased electronic conductivity, diffusion efficiency, and kinetic properties of Co_3O_4 during the lithiation and delithiation process. This material shows promising potential for use in high-rate anodes for lithium-ion batteries.

1. Introduction

Rechargeable lithium-ion batteries (LIBs) have been widely applied to various portable electric and electronic devices. Carbonaceous material graphite has been used as the main commercialized negative electrode material for LIBs due to its low cost, high safety, non-toxicity, low operating voltage, and good cycling stability.[1] However, the low Li-storage capacity and Li-ion diffusion coefficient of this material limit its wider applications.[1-2] Many studies have tried to find new appropriate materials to substitute for conventional carbonaceous material. As a new class of negative electrode materials, transition metal oxides have been investigated as promising negative electrode materials for LIBs.[3-7] The lithium storage mechanisms and characteristics of transition metal oxide materials have been distinctly demonstrated to exhibit various advantages, such as very high capacity, widespread availability, good stability, and environmental benignity. Additionally, they can deliver as high as three times more the capacity of currently used carbonaceous graphite. As an important p-type semiconductor, nanostructured cobalt oxide (Co_3O_4) has been extensively studied owing to its potential applications such as in gas sensors,[8-9] catalysts,[10-11] solar energy absorbers,[12] field emission devices,[13] magnetic materials,[14] and supercapacitors.[15-16] In addition, Co_3O_4 is also regarded as a promising alternative anode material for LIBs due to its high theoretical capacity (890 mAh g^{-1}). In principle, it can store more than eight lithium ions per formula unit during charge/discharge.[17] However, the major limiting factors of Co_3O_4 are its poor electrical conductivity and large volume expansion/contraction as well as severe particle aggregation associated with the Li^+-insertion and extraction process, which ultimately lead to electrode pulverization and the loss of interparticle connectivity.[18] This results a large irreversible capacity loss and poor cycling stability.[4,19] It is well recognized that the particle size, morphology, and structure of electrode materials play crucial roles in determining electrochemical performances.[20] Until now, several methods and strategies have been developed to prepare Co_3O_4 and solve these problems, including the use of carbon based nanocomposites[21-22] and increasing the specific surface area by preparing nanoparticles with various morphologies and dimensions.[23-30] However, to maintain high reversible capacity combined with high coulombic efficiency, long cycling stability and superior rate capability of Co_3O_4 electrode material still remains a challenging issue.

In the present work, a novel strategy to improve the electrochemical performance of Co_3O_4 nanostructure by potassium ion (K^+) doping is reported. The interest in K^+-doped Co_3O_4 is derived from various reasons. Most importantly, potassium (K) is the most effective additive for the Co_3O_4, which significantly improved the catalytic activity of Co_3O_4 for direct decomposition of N_2O and soot combustion under loose contact.[31-32] It was also found that the catalytic activity was fully

dependent on the amount of K in both the above mentioned cases.[33] Therefore, the optimized K^+-doped Co_3O_4 nanocomposite was synthesized using a cost-effective precursor and low-temperature facile solvothermal method in polyol medium. The polyol process has many advantages since it allows for nanoscale synthesis at lower synthesis temperatures and short-term heat treatment. Electrochemical tests demonstrate that the K^+-doped Co_3O_4 could exhibit high charge/discharge capacity, long cycleability and high rate capability without noticeable capacity fading. For comparison, undoped Co_3O_4 was also investigated. This strategy features facile procedure with a novel dopant for realizing the large-scale production of Co_3O_4 nanoparticles with improved electrochemical performances.

2. Experimental

2.1 Material synthesis

Undoped and K^+-doped Co_3O_4 samples were successfully synthesized by solvothermal method in polyol medium.[34-35] Cobalt (II) nitrate hexahydrate [$Co(NO_3)_2.6H_2O$, 98%, Sigma-Aldrich, USA] and potassium nitrate [KNO_3, 99.999%, Sigma-Aldrich, USA] were used as precursor materials. Ethylene glycol (EG) [$HOCH_2CH_2OH$, 99%, Dae-Jung Chemicals, South Korea] was used as a solvent. In a typical synthesis, the calculated amount of $Co(NO_3)_2.6H_2O$ was mixed into 30 ml of EG solvent and stirred until a clear solution was obtained. A calculated and optimized amount of KNO_3 (8 wt%) was then added to the obtained solution and stirred for 5 h to obtain a clear suspension. The resulting solution was sealed in a 40-ml Teflon-lined bomb and kept for 16 h in a drying oven pre-heated at 180 °C. After cooling and ultrasonication, the resulting precipitates were washed by acetone several times to remove residual organic constituents before filtering using ceramic membrane funnels and drying in a vacuum chamber for 12 h at 120 °C. The obtained sample was thoroughly ground using an agate mortar and annealed at 400 °C for 5 h in air to increase the crystallinity of the sample. The undoped Co_3O_4 sample was synthesized and annealed under the same conditions without the addition of KNO_3 for comparison. The final annealed samples were used to investigate the electrochemical performances.

2.2 The structure and morphology characterizations

The structures of annealed samples were identified by synchrotron X-ray powder diffraction data, which was collected at the 9B high-resolution powder diffraction beamline of the Pohang Accelerator Laboratory, South Korea. The incident X-rays were monochromatized to the wavelength of 1.54740 Å by a double-bounce Si (111) monochromator. The surface morphology and particle sizes were analyzed by field-emission scanning electron microscopy (FE-SEM, S-4700 Hitachi) and field-emission transmission electron microscopy (FE-TEM, Philips Tecnai F20 at 200 kV, KBSI, Chonnam National University, South Korea). For FE-TEM characterization, the samples were first dipped in ethanol and dispersed by ultrasonic vibration before coating onto copper grids. The EDX mapping was done on a Hitachi S-4700 FE-SEM equipped with an energy-dispersive X-ray analyzer (EMAX Energy EX-200, Horiba). The thermogravimetric analysis (TG) of annealed powders were performed in an argon atmosphere using TA instrument-SDT Q 600 from room temperature to 1000 ºC at a heating rate of 5 ºC/min.

2.3 Electrochemical measurements

The working electrodes were prepared by mixing the active material, super-P, and polyvinylidene fluoride binder with a weight ratio of 8:1:1 in N-methyl-2-pyrrolidone solvent to form a slurry. The resulting slurry was then coated onto a copper foil current collector and dried under vacuum at 80 °C overnight. The slurry was punched into circular electrodes after pressing between stainless steel twin rollers, in order to improve the contact between the active material and copper foil. The electrolyte used was 1 M $LiPF_6$ dissolved in a mixture of ethylene carbonate and dimethylcarbonate (1:1 in volume ratio). The 2032 coin-type cells were assembled in a glove box under a dry argon atmosphere using lithium metal as a reference electrode, and a polymer membrane together with glass fiber as a separator. The coin cells were kept in the glove box for 12 h for aging before electrochemical measurements. The cyclic voltammogram (CV) test was carried out on both the samples at a scan rate of 0.1 mV s^{-1} in the range of 0.0-3.0 V vs. Li/Li^+ by using Bio Logic Science Instrument (VSP 1075). Galvanostatic testing (BTS–2004H, Nagano, Japan) was used to investigate the electrochemical performance over the potential range of 0.005-3.0 V vs. Li^+/Li at different current rates. For doing ex-situ TEM studies, the cycled electrodes were initially dissociated from the cell in an argon filled glove box. The electrodes were then washed thoroughly with the solvent, dimethyl carbonate to remove the electrolyte. Then, they were dried at 80 °C in a vacuum oven for overnight. For ex-situ TEM studies, the electrode material is scraped off from the Cu-substrate and the powder is recovered inside the glove box. These materials were then dispersed in ethanol using ultrasonic vibration. A drop of suspension was deposited on copper grids. Electrochemical impedance spectroscopy (EIS) measurements were carried out on a Bio Logic Science Instrument (VSP 1075) to measure the electronic conductivities of the assembled cells. Before the measurement, the cells were cycled for 5 cycles and then measured at frequency ranging from 0.01 Hz to 1.0 MHz. A small AC signal of 5 mV amplitude was used for perturbation of the system throughout the tests.

3. Results and discussion

3.1 The crystal structure and morphology

Figs. 1 (a) and (b) shows the Synchrotron XRD patterns of K^+-doped and undoped Co_3O_4 samples, respectively. Both the patterns exhibit identical XRD patterns and could be exactly indexed to spinel Co_3O_4 (JCPDS card no. 65-3103), with cubic structure and space group of *Fd3m* (227). No extra peaks were observed, indicating that the $K_xCo_{3-x}O_{4-\delta}$ (x = 0.08) sample was a good solid solution with spinel structure, and that a small amount of the doping of K^+ ions enter the lattice of Co_3O_4 without causing any structural changes of the basic Co_3O_4 structure. More importantly, the peak shifting was also not observed in the doped sample, which clearly indicates that the K^+ ions are highly dispersed in the matrix of the Co_3O_4, similar to previously reported literatures.[32-33]

The surface morphology of both the samples was investigated by FE-SEM analysis, as shown in Fig. 2. Figs. 2 (a) and (b) show

the FE-SEM view of the K^+-doped and undoped Co_3O_4 samples, respectively. It can be clearly observed that both the samples exhibit different morphology. The K^+-doped Co_3O_4 sample shows that the primary particles are almost spherical and tend to be agglomerated, and form dense and bigger secondary particles.

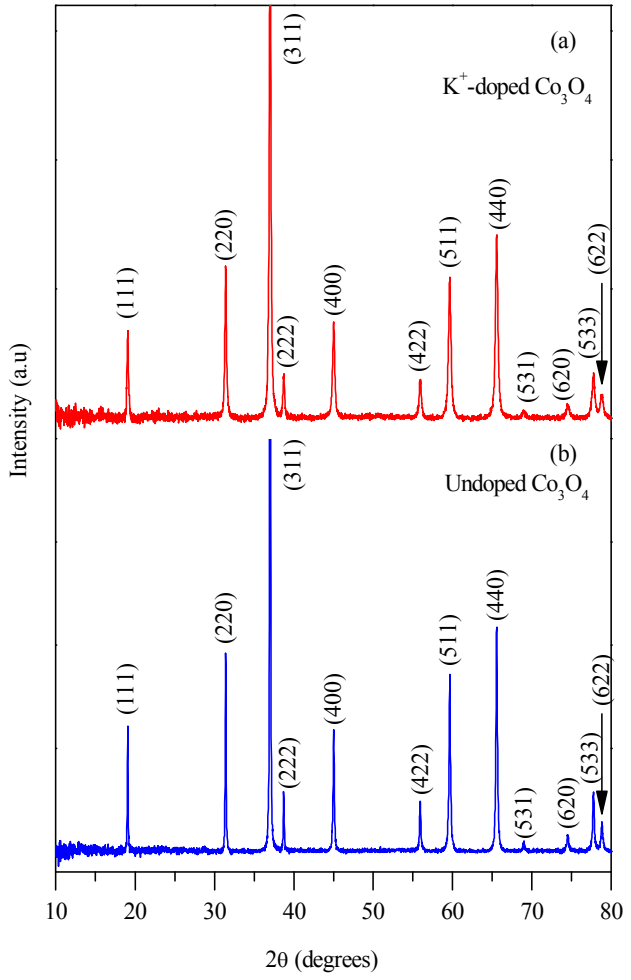

Fig. 1. Synchrotron X-ray powder diffraction patterns of (a) K^+-doped and (b) undoped Co_3O_4 sample.

Furthermore, in the case of undoped Co_3O_4, the nanoparticles are agglomerated and connected to each other. However, the large agglomerated nanostructure participates in a conversion mechanism that could be detrimental to electrochemical performances. It may be reasonable to suggest that K^+ ion as a dopant help to reduce the agglomeration and particles linkage with each other. In order to further determine the internal structure and existence of K^+ ions in the doped Co_3O_4 sample, we carried out elemental mapping and EDX characterization of the K^+-doped Co_3O_4 sample, as shown in Fig. 2 (c). In the mix EDX mapping, the results confirmed that the K element (marked as red colour) was indeed uniformly distributed on/in Co_3O_4 sample (Co was marked as green colour). The K signal is quite weaker in the mapping, which is in accordance with small stoichiometric precursor amount of KNO_3. The inset of Fig. 2 (c) shows the EDX spectrum of K^+-doped Co_3O_4 sample. The only peaks of K, Co, and O are obviously identified without any other impurity peaks, indicating the clear existence of K^+ ions in the sample with high purity.

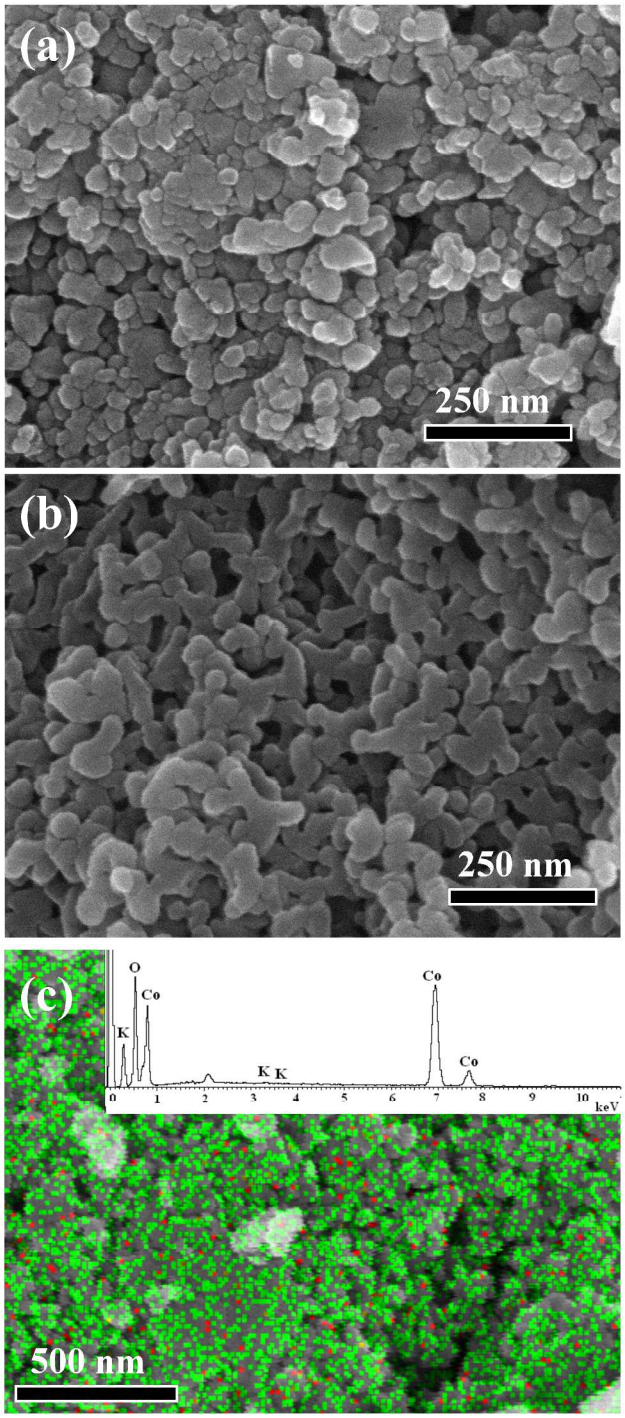

Fig. 2. FE-SEM images of (a) K^+-doped and (b) undoped Co_3O_4 samples. (c) Mix elemental mapping of K (red colour) and Co (green colour) in the K^+-doped Co_3O_4 sample. The inset of Fig. 2 (c) shows the EDX spectrum of same K^+-doped Co_3O_4 sample.

In order to further investigate the effect of K^+ doping on the Co_3O_4 morphology, FE-TEM and HR-TEM images were also carried out. Figs. 3 (a) and (c) show the FE-TEM images of the K^+-doped and undoped Co_3O_4 samples, respectively. There is no

big significant change in both the structure and morphology of the undoped and doped samples.[36] The primary particle sizes are in the range of 25-50 nm for both the samples. The FE-TEM image of the K^+-doped and undoped Co_3O_4 samples also reveals that both products have aggregations of some of the primary Co_3O_4 nanoparticles due to their small dimensions and high surface energy. More importantly, the primary undoped Co_3O_4 nanoparticles are clearly connected with each other in the FE-TEM observation and are in agreement with the observed FE-SEM result. Nanoparticles of the Co_3O_4 are also very important for better electrochemical performance, as they provide large surface area with reduced mass and charge diffusion distances for rapid electrochemical reactions. To gain structural information, HR-TEM imaging was also performed on the edges of nanoparticles and the results are displayed in Fig. 3 (b) and (d) for K^+-doped and undoped Co_3O_4 samples, respectively.

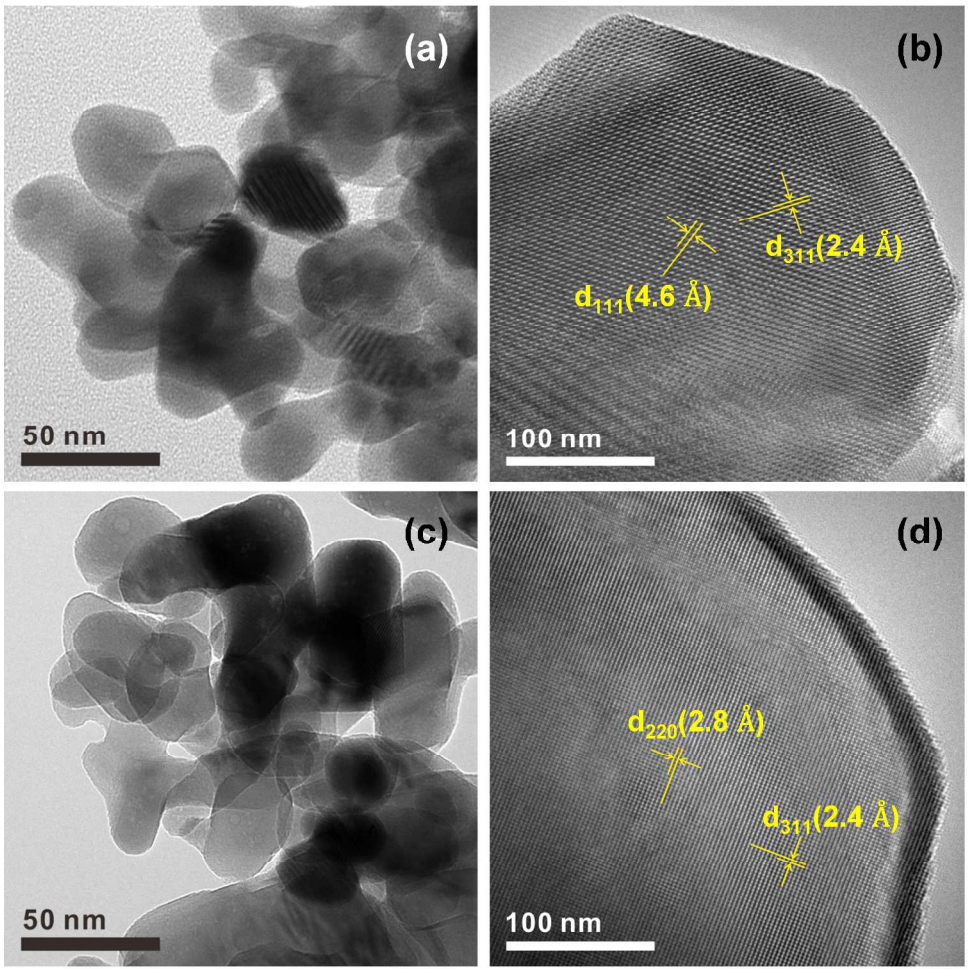

Fig. 3. FE-TEM and HR-TEM images of K^+-doped Co_3O_4 nanoparticles (a and b) and undoped Co_3O_4 nanoparticles (c and d) respectively.

Both products indicate high crystallinity with distinct lattice fringes. From the HR-TEM images, lattice fringes having interplanar d-spacings of 4.6 Å and 2.4 Å for doped sample, and 2.8 Å and 2.4 Å for undoped Co_3O_4 sample, agrees well with the lattice planes of (111), (311), (220) and (311) of Co_3O_4 crystals.

3.2 Electrochemical performance

In order to understand the effect of K doping on the electrochemical performance of the Co_3O_4, CV tests were carried out. Fig. 4 illustrates the initial three CV cycles of the K^+-doped and undoped Co_3O_4 samples in the potential window of 0.0-3.0 V. It can be clearly observed that both the samples exhibit similar shapes and curve area, indicating similar redox reactions take place in the electrodes. The first CV curve differs from the subsequent CV curves. In the first scan, the main irreversible cathodic peak is observed at 0.80 V for the K^+-doped Co_3O_4 electrode and at 0.83 V for the undoped Co_3O_4 electrode, corresponding to the initial reduction of Co_3O_4 to Co, the electrochemical formation of amorphous Li_2O ($Co_3O_4 + 8Li^+ + 8e^- \rightarrow 4Li_2O + 3Co$), and the decomposition of electrolyte to form a solid electrolyte interphase (SEI) layer at the interface between the electrode and electrolyte. The observed dominant anodic peak in the first scan at 2.0 V for K^+-doped and 2.1 V for the undoped Co_3O_4 samples, can be ascribed to the reversible oxidation reaction of metal Co to Co_3O_4. During the successive cycles, the cathodic peaks shift to a higher potential of about 1.1 V while the anodic peaks position remain almost unchanged (at 2.1 V), indicating the reversible reduction and oxidation of Co_3O_4. However, the positive shift of cathodic peaks in the subsequent cycles can be ascribed to the polarization of the electrode in the

first cycle. More importantly, the peak intensity and integral areas of the third cycle are close to that of the second one for K^+-doped Co_3O_4, but are obviously decreased for the undoped Co_3O_4, indicating that the electrochemical reversibility of K^+-doped Co_3O_4 is gradually established after the initial cycle and is much better than that of undoped Co_3O_4.

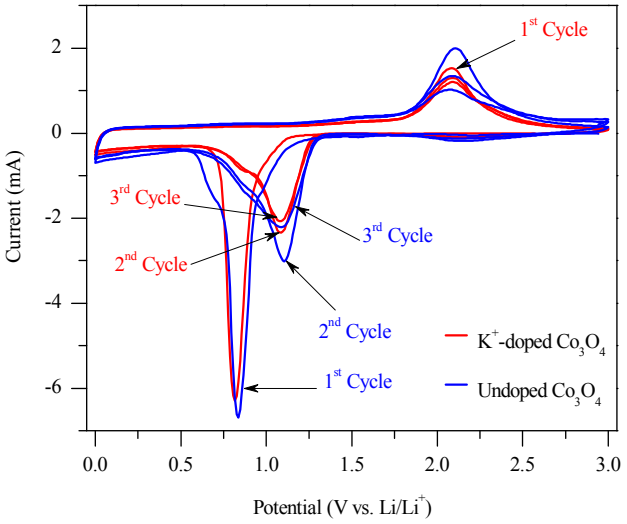

Fig. 4. Cyclic voltammograms of the K^+-doped and undoped Co_3O_4 samples.

Fig. 5 shows the electrochemical performance of K^+-doped and undoped Co_3O_4 electrodes at the constant current rate of 89 mA g^{-1} (corresponding to ~0.1 C) between the voltage range of 0.005–3.0 V vs. Li^+/Li. Figs. 5 (a) and (b) show the typical 1st, 2nd and 5th charge/discharge curves of the K^+-doped and undoped Co_3O_4 electrodes respectively. The charge/discharge profile in the first cycle is different from that in the following cycles due to the electrolyte decomposition and SEI layer formation.[4] In the first discharge step, both the electrodes exhibited two well-defined voltage plateaus at around ~1.2 and 1.1 V, and then the plateaus changes to a sloping curve down to the cut-off voltage of 0.005 V. This is due to the reduction process of Co_3O_4 to CoO and then the metallic Co, respectively, along with the formation of SEI layers, which can cause the irreversible capacity loss.[37] Note that, the high voltage plateau at 1.2 V is only observed for the nanostructured Co_3O_4 with high specific surface area. In the following discharge processes, the long voltage plateau shifts to higher potentials (as observed in the CV). In the initial charge process, there appears a main voltage plateau at about 2.0 V, corresponding to the reversible oxidation of Co_3O_4 and the decomposition of Li_2O matrix.[38] Therefore, the electrochemical reaction mechanism of Co_3O_4 with Li is different from classical Li insertion/de-insertion in layered materials, and involves the formation and decomposition of Li_2O accompanying the reduction and oxidation of cobalt nanoparticles. As shown in Figs. 5 (a) and (b), the first discharge and charge capacities are 1208.9 and 931.8 mAh g^{-1} for K^+-doped Co_3O_4 and 1240.0 and 952.4 mAh g^{-1} for undoped Co_3O_4 electrode, respectively. However, the low initial coulombic efficiency (~77%) in both the electrodes may have resulted from the irreversible conversion reaction and the formation of an SEI layer. More importantly, the difference in the open circuit voltages (OCV) of the doped sample (~2.5 V) and the undoped sample (~2.8 V), also indicating a clear effect of K insertion in the doped sample.

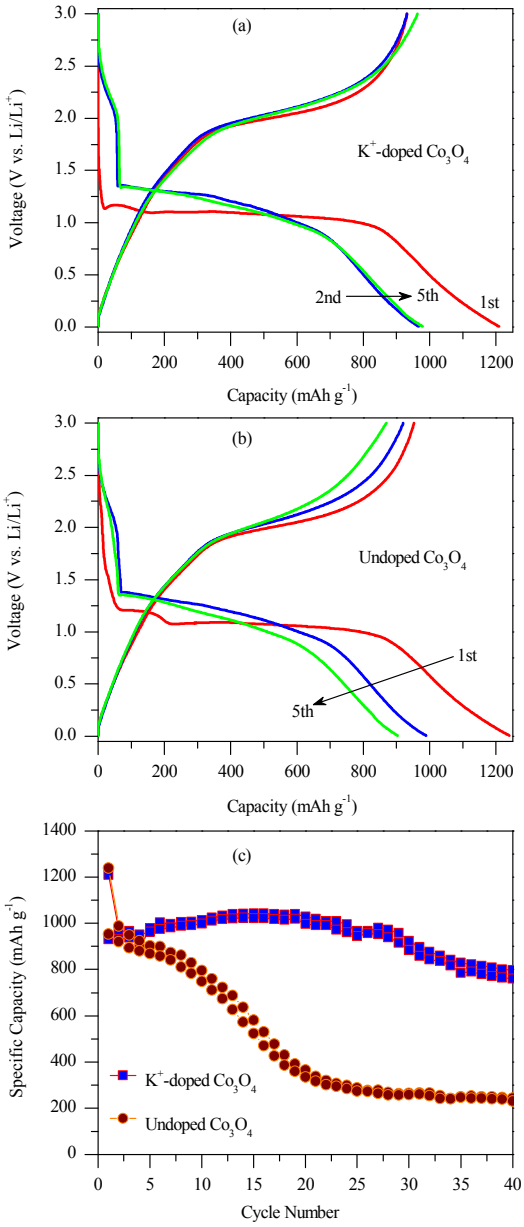

Fig. 5. Discharge/charge curves of (a) K^+-doped Co_3O_4; (b) undoped Co_3O_4 electrode recorded at constant rate of 0.1 C and (c) the cycling performance of same electrodes.

Moreover, the K^+-doped Co_3O_4 electrode exhibited reversible charge capacities of 931.8 mAh g^{-1} at the 2nd cycle, and 963.1 mAh g^{-1} at the 5th cycles. The shapes of the profiles are not altered after the first cycle, indicating excellent stability of the doped electrode as an anode for LIBs, and suggesting enhanced electrochemical lithium storage performance. In addition, the coulombic efficiency rapidly increases from 77% in the first cycle to ~98% in the 5th cycle, and remains almost same in the

following cycles. The reason could be that the K doping improves the electrical conductivity and kinetic properties during lithiation and delithiation, which provides a larger active surface area than that of the undoped sample, and the formation of K_2O may also facilitate the alleviation of the mechanical stress induced by volume changes during repeated charge/discharge cycles.[36] The charge capacities of the undoped Co_3O_4 nanoparticle electrode significantly drop down to 920.1 mAh g^{-1}, and 868.5 mAh g^{-1} after 2nd and 5th cycles, respectively, which can be attributed to the pulverization and the aggregation of the Co_3O_4 nanoparticles and the consequential reduction of electrical contacts between them. The overall electrochemical reaction mechanism of undoped Co_3O_4 and K^+-doped Co_3O_4 with Li can be expressed by following equations respectively based on the reported literature[36]:

$$Co_3O_4 + 8Li^+ + 8e^- \leftrightarrow 3Co + 4Li_2O \quad \text{(i)}$$

$$K_xCo3-xO4-\delta + (8-x)Li^+ + (8-x)e^- \leftrightarrow (3-x)Co + \frac{\delta - x}{2} Li2O + \frac{x}{2} K2O \quad \text{(ii)}$$

Fig. 5 (c) displays the cycling performance of the electrodes made from K^+-doped and undoped Co_3O_4 nanoparticles at a constant current density of 89 mA g^{-1} (corresponding to ~0.1 C). A charge capacity of 931.8 mAh g^{-1} was achieved for the K^+-doped Co_3O_4 electrode in the first cycle. It can be seen that the reversible capacity of nanostructured K^+-doped electrode experiences a gradual increase in the initial fifteen cycles and stabilizes at 760.1 mAh g^{-1} after 40 discharge/charge cycles, which is almost ~82% retention of the initial charge capacity. Similar capacity rising phenomena for the initial few cycles have been also observed from transition-metal oxides anode materials due to the formation of polymeric surface film attached to the active material.[5,39] In addition, the obtained capacity of doped electrode is still much higher than the theoretical capacity of commercial graphite-based anode materials (372 mAh g^{-1}). However, the undoped Co_3O_4 nanoparticle electrode showed a first charge capacity of 952.4 mAh g^{-1}, and in the following cycles, the capacity faded rapidly to only 229.7 mAh g^{-1} after 40 charge/discharge cycles and retained only 24% of the initial one. Clearly, the K^+-doped Co_3O_4 nanoparticle electrode exhibited much better capacity retention than the undoped nanoparticle electrode. It is believed that the K^+ ion plays an important role because it can improve the electronic conductivity, decrease the Ohmic loss, and further provide electronic conduction pathways in the doped sample. It may be also reasonable to suggest that the presence of K^+ ions, making the Li^+ ions transfer quickly and efficiently at the interface, which greatly enhances the reactivity of the electrode reaction. The better lithium storage capability of the K^+-doped Co_3O_4 electrode sheds light on the potential application as an anode material in LIBs. This could be extended to other metal oxide anode materials used in LIBs applications.

In order to understand the effect of K^+ ion on the electrochemical properties of Co_3O_4 nanoparticles, we examined their morphology change after electrochemical cycling. For doing ex-situ TEM studies, both the cycled electrodes were recovered in the glove box at room temperature and processed as mentioned in the experimental section (2.3). Figs. 6 (a) and (b) show the ex-situ TEM images of K^+ doped and undoped Co_3O_4 electrodes, respectively. Both the electrodes exhibited different morphology. The better cycling response of K^+-doped Co_3O_4 electrode is well supported by the corresponding ex-situ TEM image, which shows that the active materials appear more compact, less defined and comprised of small nano-crystalline regions. More importantly, it can be clearly seen that the active material is still highly dispersed or embedded in the amorphous regions of mainly Li_2O.[40-41] Further, it is well established that electrolyte decomposition and SEI film formation takes place on the surface of the active material and may contribute to the amorphous region observed in the ex-situ micrographs. In addition, the grain size reduction of the embedded particles in an amorphous matrix is due to the so-called "electrochemical grinding" effect.[42] However, it may be possible that K doping acts as a buffer zone that accommodates the volume expansion/contraction in the doped electrode during charge/discharge cycling. The structure and conducting network of the electrode remains unchanged and the cycling performance is thus improved. As anticipated, the undoped Co_3O_4 electrode suffers from severe volume changes and mechanical damage with increasing cycle numbers. This reasoning is well supported by observing the corresponding ex-situ TEM image in Fig. 6 (b). However, the image shows that the active material phase was destroyed during the cycling and appears not to be embedded into the matrix. It may be possible that the active material was peeled off from the current collector during extended cycling. This pulverization of active materials degrades the mechanical stability of the electrode and probably causes degradation of the undoped Co_3O_4 electrode.

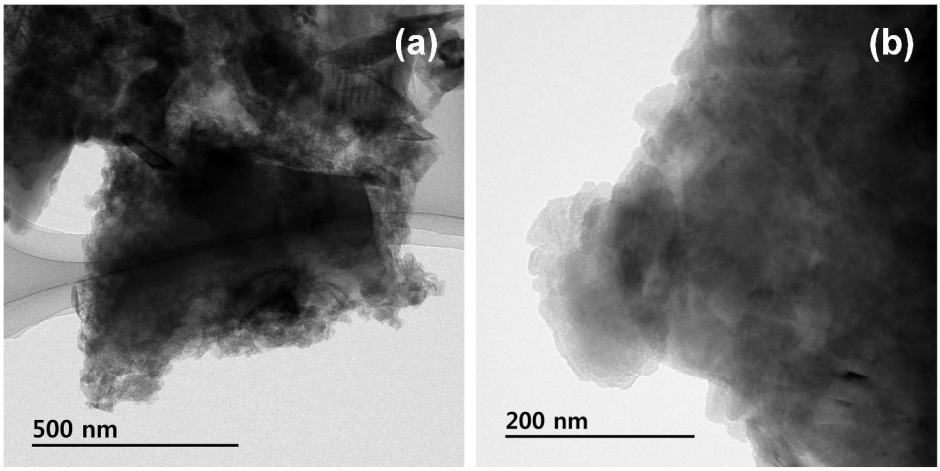

Fig.6. FE-TEM images of (a) K^+-doped Co_3O_4 electrode and (b) undoped Co_3O_4 electrode after 40 charge/discharge cycles.

Fig. 7 presents the schematic illustration of K^+ doped Co_3O_4 spinel structure. Generally, in the structure of Co_3O_4, the cation Co^{2+} occupies the tetrahedral (*8a*) site (A) and Co^{3+} ions occupy the octahedral (*16d*) site (B), i.e. $(Co_1^{2+})_A(Co_2^{3+})_BO_4$. In the reported literatures of Li^+-doped Co_3O_4 samples, Rasiyah and Nikolov suggested that Li^+ ion may enter in the tetrahedral or octahedral sites and the extra charges could be compensated by excess Co^{3+} ion in the tetrahedral sites, i.e $[(Li_x^+Co_{1-2x}^{2+}Co_x^{3+})_A(Co_2^{3+})_BO_4]$ or some Co^{4+} ions in the octahedral sites i.e $[(Co_1^{2+})_A(Li_x^+Co_{2-x}^{3+}Co_x^{4+})_BO_4$.[43-44] This study also reported that the distribution of Li^+ ion in the tetrahedral and octahedral sites of spinel lattice was also influenced by the synthesis temperature. However, due to the unfavorable condition for the formation of Co^{4+} ion at low reaction temperatures in air atmosphere or larger ionic radii of the guest ion lead us to conclude that K^+ ion may preferentially occupy the tetrahedral sites in the prepared Co_3O_4 spinel.[45] Further, the variations of the peaks positions in the initial CV cycles (Fig 4) between doped and undoped samples and OCV potential change in charge/discharge confirms the enhancement in Co^{3+} amount in A site with higher content of K^+ doping.[45]

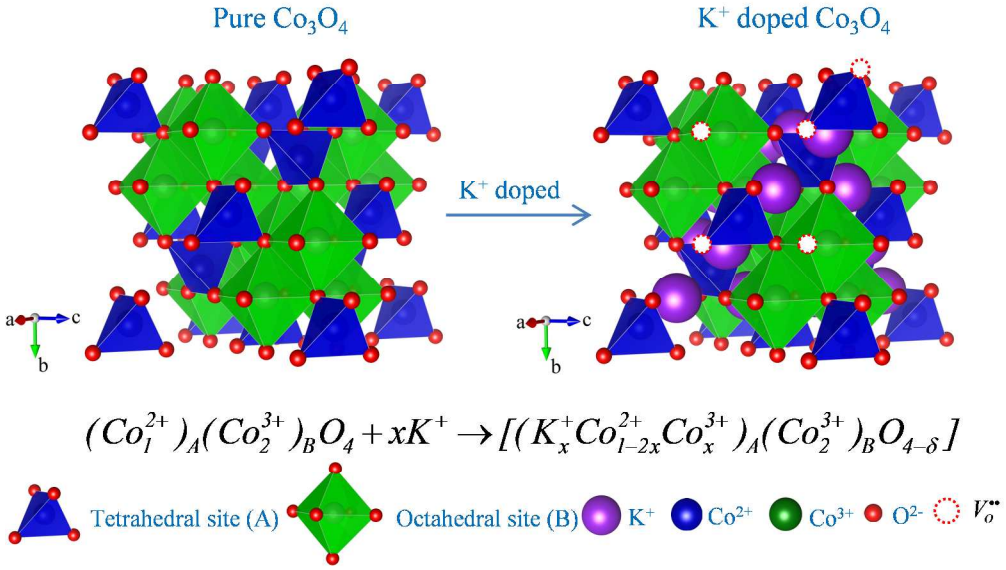

Fig. 7 The schematic illustration of K doping into spinel structure of Co_3O_4.

In the doped sample, when the K^+ ions are inserted into the lattice of Co_3O_4, the difference in ionic radii between K^+ ion (1.38 Å) and Cobalt ions (Co^{2+} : 0.78 Å, and Co^{3+} : 0.64 Å) result in the lattice deformation of Co_3O_4. The strain energy due to the lattice deformation slightly causes the dislocations and imperfections in the spinel crystal structure. In addition, the formula ($K_xCo_{3-x}O_{4-\delta}$; x = 0.08) also indicates that the 8 wt% of potassium (K) ions are inserted into the lattices and in order to maintain the charge neutrality, some oxygen vacancies ($V_O^{\bullet\bullet}$) are created in the system. In addition, Y. Guo et.al had also reported that due to the interactions between K and Co_3O_4 the distorted Co_3O_4 nanocrystals weakened the Co–O bonds, and consequently improved the activity of lattice oxygens and accelerate the formation of active O^-.[32] Therefore, it can be concluded that due to the above mentioned reasons, the doped sample may exhibit higher electronic conductivity, which eventually improves the electrochemical properties.

The TG curves of the annealed K^+-doped and undoped Co_3O_4 samples is depicted in Fig. 8 (a). The thermal analysis was carried out in the argon atmosphere. It can be clearly seen that both the curves shows only one significant weight loss at > 800 °C, which correspond to the decomposition of Co_3O_4 to CoO with a slight amount of oxygen loss according to the equation given below;[38]

$$Co_3O_4 \rightarrow 3CoO + \frac{1}{2}O_2 \qquad \text{(iii)}$$

However, to further confirm the decomposition of Co_3O_4 to CoO in the TG analysis, Fig. 8 (b) shows the typical representative powder XRD pattern of K^+-doped Co_3O_4 sample after TG measurement, which can be exactly indexed to pure CoO phase (JCPDS card no. 75-0533) without any impurities. In addition, the endothermic reaction temperature (> 800 °C) in the K^+-doped Co_3O_4 powder is slightly (~2 wt%) lower compared to the undoped Co_3O_4 powder, and this must be due to the small primary particle sizes of k-doped Co_3O_4 sample and their morphological differences.[46] The inset of Fig. 8 (a) also shows the decomposition reaction of K^+-doped and undoped Co_3O_4 samples accompanied with the oxygen loss difference. More importantly, in the TG curve of K^+-doped Co_3O_4 sample, there is no any weight loss between 300-700 °C, which confirms that the potassium (K) is not evaporated separately in the form of K_2O, but exists in the solid solution limit within the lattice of Co_3O_4. In addition, in the case of K^+-doped Co_3O_4 sample, the oxygen weight loss is slightly higher (7.2 wt%) than the undoped Co_3O_4 sample (6.6 wt%), which not only confirms the existence of potassium but also the difference in the cobalt valence states due to charge compensation in the doped sample compared to that in the undoped or K-free sample. In addition, OCV is lower in the case of doped sample, which clearly indicates that K^+ ion is only

inserted instead of substituting the cobalt ion in Co_3O_4. In order to account for K charge compensation, the average oxidation state of cobalt is slightly reduced, which results in a lower OCV for the doped sample. Author's believed that the K^+ ions reside close to the lattice and play the role of a pillar without causing any major structural lattice distortion and thereby promote more facile Li^+-insertion/de-insertion in the doped sample compared to that in the undoped sample.

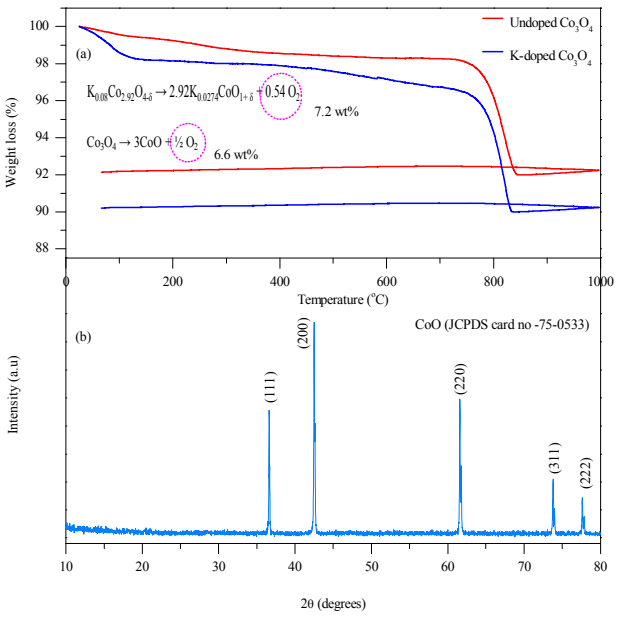

Fig. 8 Thermogravimetric analysis of annealed K^+-doped and undoped Co_3O_4 powders in argon atmosphere.

Beside charge/discharge and cycleability, the electrodes rate capabilities are also evaluated at various current rates between 0.1 C to 3 C (1 C = 890 mA g^{-1}) to examine the effectiveness of K doping, as can be seen in Fig. 9.

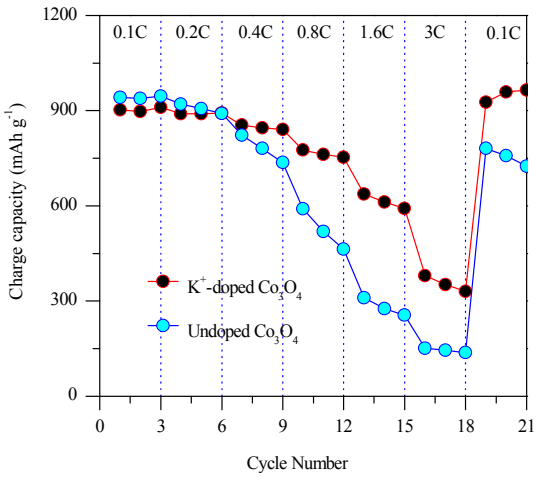

Fig. 9 The comparsion of rate capability of K^+-doped and undoped Co_3O_4 at various current rates between 0.1 and 3 C.

It can be observed that the K^+-doped Co_3O_4 electrode displays much better electrochemical activity than the undoped Co_3O_4 electrode. For example, when the current rate was first increased from 0.1 C to 0.2 C and then 0.4 C, the K^+-doped Co_3O_4 electrode can still maintain a reversible charge capacity of 845.4 mAh g^{-1}, whereas the capacity significantly reduced to 737.1 mAh g^{-1} in the case of undoped Co_3O_4 electrode. The following reversible capacity of the K^+-doped Co_3O_4 was comparatively slowly lowered to 761.9 mAh g^{-1}, 612.2 mAh g^{-1}, and 351.3 mAh g^{-1} under 0.8 C, 1.6 C, and 3 C respectively, while that of undoped Co_3O_4 electrode showed only 519.3 mAh g^{-1}, 276.1 mAh g^{-1}, and 144.2 mAh g^{-1} under the same current rates. In addition, when the current rate was again returned back to 0.1 C, the K^+-doped Co_3O_4 electrode resumed almost the same reversible capacity which was achieved initially. It may be reasonable to assume that the K^+ ions facilitate more of the Li^+ ions insertion/deinsertion in the doped electrode and enhances the kinetics and the extent of electrode reactions. The obtained electrochemical results demonstrate that the obtained K^+-doped Co_3O_4 electrode is excellent in performance compared with that of the undoped Co_3O_4 electrode.

The K^+-doped Co_3O_4 electrode's enhanced electronic conductivity was further verified by EIS measurements. Both electrodes are investigated after 5 charge/discharge cycles and the results are shown in Fig. 10. It is clear that the impedance responses of the K^+-doped Co_3O_4 cell differ from the undoped Co_3O_4 cell. In both the case, the EIS curves are composed of a depressed semicircle at the high to intermediate frequency range, and there is a straight line at lowest frequency region. As can be seen from Fig. 10, the impedance fitting was performed by EC-lab software and the corresponding equivalent circuit is also shown in the inset of figure. The parameters R_1, R_2 and Z_w in the circuit correspond to the ohmic resistances of the electrolyte, Li^+ ion charge transfer and the Warburg impedance, respectively. Generally, it is well-known that the high frequency semicircle and the semicircle in the medium frequency region are related to the SEI film and/or contact resistance and the Li^+ ion charge transfer impedance at the electrode/electrolyte interface, respectively. The sloping line at the low frequency end corresponds to lithium diffusion processes within the electrode and is known as the Warburg impedance.[47-48] However, the smaller the charge transfer resistance, the smaller the diameter of the semicircle. The results of fitting analysis indicate that the R_{ct} value (18.12 Ω) for K^+-doped Co_3O_4 electrode is much smaller than the value of undoped Co_3O_4 electrode (128.8 Ω), indicating that K^+ doping is favorable to improve the electronic conductivity. Furthermore, the values of R_1, Z_w and Q_1 of K^+-doped Co_3O_4 electrode also show the smallest values than those of the undoped sample. Moreover, the increased slope in the low frequency end for the K^+-doped sample demonstrates that K^+ ion doping can improve Li^+ ion migration in Co_3O_4 and exhibit the better electrochemical performance.[49]

Conclusions

In summary, the undoped and K^+-doped Co_3O_4 ($K_xCo_{3-x}O_{4-\delta}$; x = 0.08) samples were successfully synthesized by a simple and low-cost solvothermal method in polyol medium, followed by annealing at a low temperature of 400 °C for 5 h. The XRD patterns show that K^+ ion has inserted into the lattice of Co_3O_4 without altering the original structure. The primary particle sizes are in the range of 25-50 nm for both the prepared samples. The

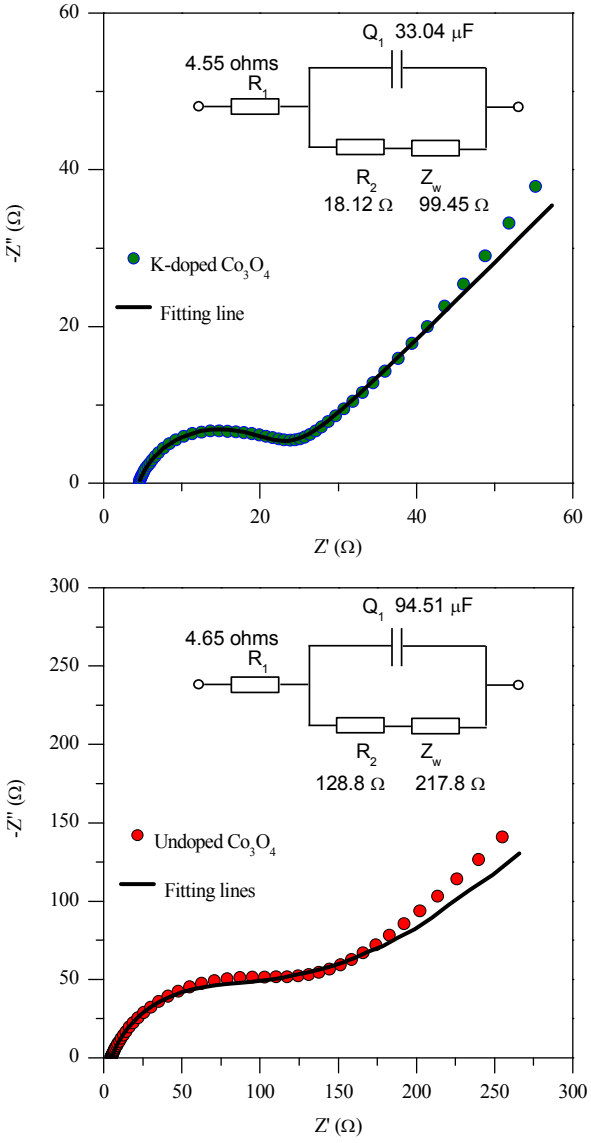

Fig. 10 The EIS plots of the K^+-doped and undoped Co_3O_4 electrodes.

K doping significantly improved the conductivity and electrochemical performance of the Co_3O_4 material compared to the undoped Co_3O_4 electrode. Precisely, the K^+-doped Co_3O_4 electrode exhibited a high specific capacity of 760.1 mAh g^{-1} at 0.1 C after 40 cycles, but in spite of this, it also retained 351.3 mAh g^{-1} at a high current rate of 3 C, which is much higher than that of undoped Co_3O_4 (only 144.2 mAh g^{-1} at 3 C). Author's believed that the electronic conductivity and lithium ion diffusivity of the K^+-doped Co_3O_4 sample are much higher compared to undoped Co_3O_4 sample. However, K^+ ion doping is beneficial for the improvement of the high-rate capability of the Co_3O_4. In addition, the presence of K_2O can also alleviate the volume changes during charge/discharge cycling.

Acknowledgement

This work was supported by the Basic Research Laboratories (BRL) Program (No. 2009-0085441) of the National Research Foundation of Korea (NRF) funded by the Ministry of Science, ICT & Future Planning. This research was also supported by Basic Science Research Program through the National Research Foundation of Korea (NRF) funded by the Ministry of Education (NRF-2009-0094055).

Notes and references

Department of Materials Science and Engineering, Chonnam National University, 300 Yongbong-dong, Bukgu, Gwangju 500-757, Republic of Korea, Fax: +82-62-530-1699; Tel: +82-62-530-1703;

**Corresponding Author*

E-mail: jaekook@chonnam.ac.kr

[1]These authors contributed equally to this work.

1 J.R. Dahn, T. Zheng, Y. Liu and J.S. Xue, *Science*, 1995, **270**, 590.
2. Y. Xiao, C. Hu, and M. Cao, *Chem. Eur. J.,* 2013, **19**, 10193.
3. H. Liu, G. Wang, J. Park, J. Wang, H. Liu and C. Zhang, *Electrochim. Acta,* 2009, **54,** 1733.
4. A.K. Rai, J. Gim, L.T. Anh and J. Kim, *Electrochim. Acta,* 2013, **100,** 63.
5. A.K. Rai, L.T. Anh, J. Gim, V. Mathew, J. Kang, B.J. Paul, N.K. Singh, J. Song and J. Kim, *J. Power Sources*, 2013, **244**, 435.
6. A.K. Rai, L.T. Anh, J. Gim, V. Mathew, J. Kang, B.J. Paul, J. Song and J. Kim, *Electrochim. Acta,* 2013, **90**, 112.
7. A.K. Rai, L.T. Anh, J. Gim, V. Mathew and J. Kim, *J. Nanosci. Nanotechno.,* 2013, **13**, 1.
8. W.Y. Li, L.N. Xu and J. Chen, *Adv. Funct. Mater.*, 2005, **15**, 851.
9. D. Patil, P. Patil, V. Subramanian, P.A. Joy and H.S. Potdar, *Talanta,* 2010, **81**, 37.
10. F. Jiao and H. Frei, *Angew. Chem. Int. Ed.*, 2009, **48**, 1841.
11. C.Y. Ma, Z. Mu, J.J. Li, Y.G. Jin, J. Cheng, G.Q. Lu, Z.P. Hao and S.Z. Qiao, *J. Am. Chem. Soc.,* 2010, **132**, 2608.
12. M. Ando, K. Kadono, K. Kamada and K. Ohta, *Thin Solid Films,* 2004, **446**, 271.
13. T. Yu, Y.W. Zhu, X.J. Xu, Z.X. Shen, P. Chen, C.T. Lim, J.T.L. Thong and C.H. Sow, *Adv. Mater.,* 2005, **17**, 1595.
14. M.J. Benitez, O. Petracic, E.L. Salabas, F. Radu, H. Tüysüz, F. Schüth and H. Zabel, *Phys. Rev. Lett.,* 2008, **101**, 097206.
15. T. Zhu, J.S. Chen and X.W. Lou, *J. Mater. Chem.,* 2010, **20**, 7015.
16. F. Zhang, C.Z. Yuan, X.J. Lu, L.J. Zhang, Q. Che and X.G. Zhang, *J. Power Sources,* 2012, **203**, 250.
17. D. Larcher, G. Sudant, J. Leriche, Y. Chabre and J. Tarascon, *J. Electrochem. Soc.,* 2002, **149**, A234.
18. L. Wang, B. Liu, S. Ran, H. Huang, X. Wang, B. Liang, D. Chen and G. Shen, *J. Mater. Chem.,* 2012, **22**, 23541.
19. J. Liu, H. Xia, L. Lu and D. Xue, *J. Mater. Chem.*, 2010, **20**, 1506.
20. B. Guo, C.S. Li and Z.Y. Yuan, *J. Phys. Chem. C,* 2010, **114**, 12805.
21. H.J. Liu, S.H. Bo, W.J. Cui, F. Li, C.X. Wang and Y.Y. Xia, *Electrochim. Acta,* 2008, **53**, 6497.
22. L. Zhi, Y.S. Hu, B.E. Hamaoui, X. Wang, I. Lieberwirth, U. Kolb, J. Maier and K. *Adv. Mater.,* 2008, **20**, 1727.
23. X.Y. Xue, S. Yuan, L.L. Xing, Z. H. Chen, B. He and Y.J. Chen, *Chem. Commun.*, 2011, **47**, 4718.
24. H. Sun, M. Ahmad and J. Zhu, *Electrochim. Acta,* 2013, **89**, 199.
25. J. Wang, B. Niu, G. Du, R. Zeng, Z. Chen, Z. Guo and S. Dou, *Mater. Chem. Phys.*, 2011, **126**, 747.
26. Y. Lu, Y. Wang, Y. Zou, Z. Jiao, B. Zhao, Y. He and M. Wu, *Electrochem. Commun.,* 2010, **12**, 101.
27. X. Xia, J. Tu, J. Xiang, X. Huang, X. Wang and X. Zhao, *J. Power Sources,* 2010, **195**, 2014.
28. J. Zheng, J. Liu, D. Lv, Q. Kuang, Z. Jiang, Z. Xie, R. Huang and L. Zheng, *J. Solid State Chem.,* 2010, **183**, 600.
29. S. Xiong, J.S. Chen, X.W. Lou and H.C. Zeng, *Adv. Funct. Mater.,* 2012, **22**, 861.
30. X. Yao, X. Xin, Y. Zhang, J. Wang, Z. Liu and X. Xu, *J. Alloy Compd.,* 2012, **521**, 95.
31. M. Haneda, Y. Kintaichi, N. Bion and H. Hamada, *Appl. Catal. B: Environ.,* 2003, **46**, 473.

32. M. Sun, L. Wang, B. Feng, Z. Zhang, G. Lu and Y. Guo, *Catal. Today,* 2011, **175**, 100.
33. K. Asano, C. Ohnishi, S. Iwamoto, Y. Shioya and M. Inoue, *Appl. Catal. B: Environ.,* 2008, **78**, 242.
34. L.T. Anh, A.K. Rai, T.V. Thi, J. Gim, S. Kim, E.C. Shin, J.S. Lee and J. Kim, *J. Power Sources,* 2013, **243**, 891.
35. A.K. Rai, J. Gim, S.W. Kang, V. Mathew, L.T. Anh, J. Kang, J. Song, B.J. Paul and J. Kim, *Mater. Chem. Phys.,* 2012, **136**, 1044.
36. J. Cao, H. Liu, J. Xie, G. Cao and X. Zhao, *J. Mater. Sci. Techno.,* 2010, **26**, 669.
37. N. Yan, L. Hu, Y. Li, Y. Wang, H. Zhong, X. Hu, X. Kong and Q. Chen, *J. Phys. Chem. C,* 2012, **116**, 7227.
38. M.M. Rahman, J.Z. Wang, X.L. Deng, Y. Li and H.K. Liu, *Electrochim. Acta,* 2009, **55**, 504.
39. L. Pan, H. Zhao, W. Shen, X. Dong and J. Xu, *J. Mater. Chem. A,* 2013, **1**, 7159.
40. Y. Sharma, N. Sharma, G.V.S. Rao and B.V.R. Chowdari, *Solid State Ionics,* 2008, **179**, 587.
41. Y. Sharma, N. Sharma, G.V.S. Rao and B.V.R. Chowdari, *Adv. Funct. Mater.,* 2007, **17**, 2855.
42. S. Grugeon, S. Laruelle, L. Dupont and J.-M. Tarascon, *Solid State Sci.,* 2003, **5**, 895.
43. P. Rasiyah and ACC Tseung, *J. Electrochem. Soc.,* 1983, **130**, 365.
44. I. Nikolov, R. Darkaoui, E. Zhecheva, R. Stoyanova, N. Dimitrov and T. Vitanov, *J. Electroanal. Chem.,* 1997, **429**, 157.
45. X. Wu and K. Scott, *Int. J. Hydrogen Energy,* 2013, **38**, 3123.
46. R. Tummala, R.K. Guduru and P.S. Mohanty, *J. Power Sources,* 2012, **209**, 44.
47. A.K. Rai, L.T. Anh, J. Gim and J. Kim, *Ceram. Int.,* 2013, **39**, 9325.
48. A.K. Rai, L.T. Anh, C.J. Park and J. Kim, *Ceram. Int.,* 2013, **39**, 6611.
49. Q. Zhang, C. Zhang, B. Li, S. Kang, X. Li and Y. Wang, *Electrochim. Acta,* 2013, **98**, 146.